Optics Letters

Measurement of the radial mode spectrum of photons through a phase-retrieval method

Saumya Choudhary,[1,*] Rachel Sampson,[2] Yoko Miyamoto,[3] Omar S. Magaña-Loaiza,[4] Seyed Mohammad Hashemi Rafsanjani,[5] Mohammad Mirhosseini,[6] and Robert W. Boyd[1,7]

[1]The Institute of Optics, University of Rochester, Rochester, New York 14627, USA
[2]CREOL, The College of Optics and Photonics at UCF, Orlando, Florida 32816, USA
[3]Department of Engineering Science, The University of Electro-Communications, 1-5-1 Chofugaoka, Chofu, Tokyo 182-8585, Japan
[4]Department of Physics and Astronomy, Louisiana State University, Baton Rouge, Louisiana 70803, USA
[5]Department of Physics, University of Miami, Coral Gables, Florida 33146, USA
[6]Department of Applied Physics and Material Science, California Institute of Technology, Pasadena, California 91125, USA
[7]Department of Physics, University of Ottawa, Ottawa, ON K1N 6N5, Canada
*Corresponding author: schoudha@ur.rochester.edu

We propose and demonstrate a simple and easy-to-implement projective-measurement protocol to determine the radial index p of a Laguerre–Gaussian (LG_p^l) mode. Our method entails converting any specified high-order LG_p^0 mode into a near-Gaussian distribution that matches the fundamental mode of a single-mode fiber (SMF) through the use of two phase screens (unitary transforms) obtained by applying a phase-retrieval algorithm. The unitary transforms preserve the orthogonality of modes before the SMF and guarantee that our protocol can, in principle, be free of crosstalk. We measure the coupling efficiency of the transformed radial modes to the SMF for different pairs of phase screens. Because of the universality of phase-retrieval methods, we believe that our protocol provides an efficient way of fully characterizing the radial spatial profile of an optical field. © 2018 Optical Society of America

https://doi.org/10.1364/OL.43.006101

Laguerre–Gaussian (LG) modes, LG_p^l, characterized by the azimuthal index l (an integer that quantifies the amount of orbital angular momentum (OAM) carried by a single photon [1]) and by the radial index p (a non-negative integer that quantifies the hyperbolic momentum charge of a single photon [2]), are solutions of the paraxial wave equation in cylindrical coordinates [3]. The LG modes are orthonormal and form a complete basis set. Both the azimuthal and radial degrees of freedom are theoretically unbounded (unlike polarization, which is two dimensional). This unbounded nature is potentially useful for applications such as classical and quantum communication [4–8], including quantum key distribution (QKD) [9,10], by allowing for high-dimensional encoding, which leads to increased information capacity [11,12]. To date, most of these applications have employed the LG_0^l, i.e., the OAM modes of lowest radial order, for which efficient means of detection

and characterization are available [13–18]. The radial modes, LG_p^l, have been under-utilized for such applications because of the absence of efficient methods for detecting and measuring the radial index.

Several interferometric techniques for the sorting of LG_p^l modes based on the principle of a universal quantum sorter [19] have recently been demonstrated [20–22]. However, with a larger number of input modes, these techniques become more complicated to implement, as several such interferometers would need to be cascaded. Projective measurements can also be used to measure mode indices, and hence are also useful for performing quantum state tomography [12,23]. Projection entails mapping a specified input mode to a particular output mode (typically a Gaussian), which can then by coupled to a single-mode fiber (SMF) that selects only the fundamental Gaussian component. Previous projective measurements of radial modes have employed flattening the phase front of the incoming field [7,24], and in [25], flattening both the phase and the intensity. While the former scenario results in crosstalk due to incomplete projection of the input modes onto the SMF mode, the latter has reduced crosstalk but with a very low detection efficiency.

LG modes retain their transverse structure as they propagate through free space, through lenses and as they reflect off of mirrors. As a consequence, one cannot use these elements to losslessly project high-order radial modes onto a Gaussian. Multi-plane light conversion (MPLC), which employs a series of phase planes and propagation, has been shown to, in principle, be able to perform any arbitrary spatial transformation [26]. The MPLC concept has been used in [27] to map several LG modes to Gaussian spots at mode-index-dependent positions at the output. In [28], a similar mapping as in [27] was performed for a few LG modes by utilizing multiple scattering. However, while the former case requires several phase planes to achieve low crosstalk, the latter configuration suffers from high scattering losses (around 99%).

Here, we present a simple and easy-to-implement protocol for measuring the radial mode spectrum of an optical field by transforming high-order radial modes to the fundamental mode of a SMF. We use two phase screens (to introduce a spatially varying transverse phase structure), placed at the object plane and at the Fourier plane of a lens, respectively, to transform a particular radial mode (LG_p^0) to the fundamental mode of a SMF, assumed here to be a Gaussian (LG_0^0). The required pair of phase screens for each input mode is calculated through the use of a phase-retrieval algorithm. The transformations performed by phase screens are in principle lossless and, hence, unitary. Since all the other elements before coupling to the SMF are also unitary, the orthogonality of modes is maintained before coupling to the SMF, which guarantees that modes with radial indices other than those for which the phase screens were designed will not couple to the SMF. Thus, through our protocol, one can measure the radial index of a mode (and thereby determine the radial mode spectrum of an optical field) with negligible crosstalk.

Figure 1(a) shows a schematic representation of our projection protocol. The transformation of a LG_p^0 mode (where $p > 0$) to a Gaussian mode is an example of a "synthesis problem," as we have *a priori* knowledge of the intensity distributions in the object plane as well as the Fourier plane [29]. We use the Gerchberg–Saxton (GS) phase-retrieval algorithm, an iterative error-reduction algorithm, [30,31] to calculate the required phase screens $\Phi_1(x,y)$ and $\Phi_2(x,y)$. The SLM1, placed at the object plane of a lens, introduces a phase $\Phi_1(x,y)$ on the input field LG_p^0 [or $f(x,y)$]. At the Fourier plane of the lens, the intensity distribution becomes similar to the intensity distribution of the LG_0^0 mode [or $g(x,y)$], but with an incorrect phase profile. The SLM2, placed at the Fourier plane, subsequently introduces another phase, $\Phi_2(x,y)$, which corrects these residual phase errors and flattens the phase. As phase transformations in the absence of losses are unitary, the orthogonality of these projected modes remains preserved before the SMF. Due to restrictions on the aperture size of our SLM, we choose the first three high-order radial modes LG_p^0 with $p = \{1, 2, 3\}$ to test our protocol.
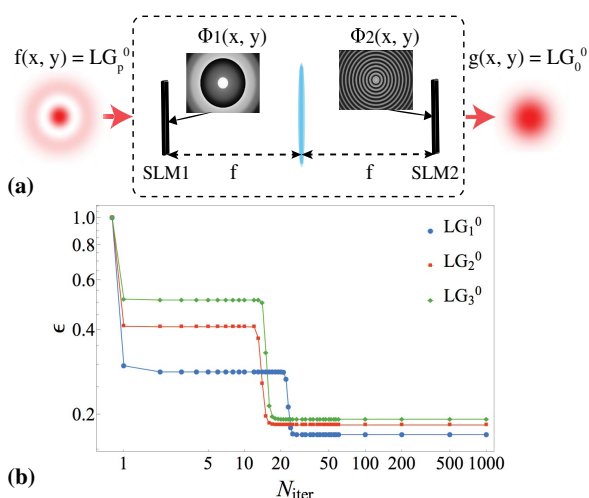
For our two-dimensional problem, the uniqueness of a phase-retrieval solution is ensured due to the non-factorability of polynomials of two-or-more complex variables [32]. We define an error metric ϵ in the Fourier domain to study the convergence of the GS algorithm to this solution with the number of iterations N_{iter}. In many cases, if a solution exists, the algorithm converges within a few iterations. However, the algorithm can also stagnate close to the local minimum of ϵ without converging any further [29]. To study the efficiency of the algorithm at calculating the required pair of phase screens for each input mode, we define ϵ in terms of C, the coherent mode-overlap efficiency between the projected LG_p^0 mode and the mode of the SMF, as follows:

$$\epsilon = 1 - C = 1 - \left| 2\pi \sum_\rho \rho F_n^*(\rho) g_n(\rho) \right|^2. \tag{1}$$

Here, ρ is the Fourier domain radial coordinate, $F_n(\rho)$ is the normalized radial mode at the Fourier plane after the application of the relevant pair of phase screens Φ_1 and Φ_2, and $g_n(\rho)$ is the desired mode at the Fourier plane (normalized Gaussian). The modes are normalized such that $2\pi \sum_\rho (\rho |F_n(\rho)|^2) = 2\pi \sum_\rho (\rho |g_n(\rho)|^2) = 1$. C also represents the fraction of input power that couples into the SMF after the phase corrections. Figure 1(b) shows the variation of ϵ with N_{iter}, where N_{iter} is the number of iterations, for the different input radial modes (LG_1^0 to LG_3^0). Without the phase corrections, or when $N_{\text{iter}} = 0$, ϵ is unity. as the unconverted high-order radial modes are orthogonal to the SMF mode. As N_{iter} increases, ϵ (C) decreases (increases) for all modes until it stagnates close to 0.18 after approximately 35 iterations. This non-negligible error represents an overall loss of power coupled into the SMF. However, as we show later in the Letter, this loss of power is not as consequential, as there is negligible crosstalk due to the preserved orthogonality of modes in our protocol [see Fig. 5(a)].

Figure 2 shows a schematic of the experimental setup used to test the protocol. Two Hamamatsu liquid-crystal-on-silicon
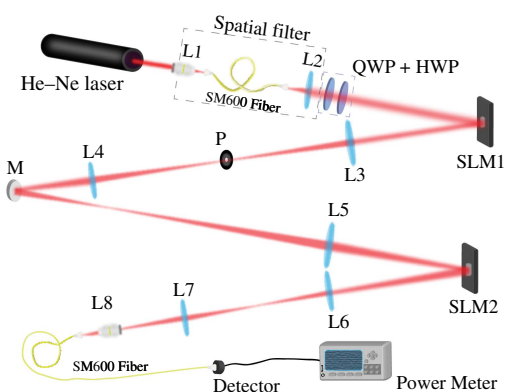

Fig. 1. (a) Schematic representation of the protocol with insets showing the phase screens, $\Phi_1(x,y)$ and $\Phi_2(x,y)$, which convert an LG_p^0 mode into a Gaussian output mode. (b) Variation of Fourier-domain error ϵ for input modes LG_1^0, LG_2^0, and LG_3^0, with the number of iterations N_{iter} of the algorithm.

Fig. 2. Schematic of the experimental setup. The labeled components are: collimating lens (L2, $f = 1$ m), microscope objectives (L1 and L8, N.A. = 0.25, 10×) to couple laser light out of and into a SMF, respectively, waveplates (QWP + HWP) to transform the polarization from the output of the fiber to the correct polarization for SLM1, pupil P [at the Fourier plane of lens L3 ($f = 1$ m)] to isolate the first order of diffraction from SLM1, and imaging systems to create a magnified image of the Fourier plane of L3 onto SLM2 [lenses L4 ($f = 125$ mm) and L5 ($f = 1$ m)] and to image the transformed field onto the exit pupil of L8 [lenses L6 ($f = 750$ mm) and L7 ($f = 1$ m)].

(LCOS) SLMs (model X10468-02), with a pixel size of 20 μm and an active area of 600 × 800 pixels, are used as the phase screens. The source is a He-Ne laser spatially filtered through the use of a SM600 fiber (single mode for 633 nm wavelength), and collimated while ensuring uniform illumination of all pixels on SLM1. The LG_p^0 modes ($p = \{0, 1, 2, 3\}$) are generated by phase-only modulation of SLM1. The amplitude and phase of the LG mode are imposed on the first order of diffraction of the grating function impressed on SLM1, in accordance with the approach given in [33]. For convenience, the first phase screen [see Figs. 3(a)–3(d)] is implemented along with the mode generation on SLM1 itself. The azimuthally averaged intensity distributions for each input radial mode at the image plane and the Fourier plane, recorded using a CCD camera, were found to differ from the theoretical intensities by a root-mean-square (rms) error of less than 10% (see Data File 1 for the actual values), thereby confirming that the generated radial modes are of good fidelity. After the second phase correction impressed by SLM2 [see Figs. 3(e)–3(h)], the transformed modes are coupled via an imaging system and a microscope objective to a SMF-coupled photodetector. Figures 3(i)–3(l) show the recorded intensities at the Fourier plane (or SLM2) of the various input modes after the application of the corresponding pair of phase screens.

The coupling efficiency of a given mode to the SMF is taken to be the ratio of the power coupled into the fiber to the total power incident on the microscope objective L8. We achieved an approximate coupling efficiency of 70% for an input Gaussian mode to the SMF through proper alignment and addition of compensating aberrations on both SLMs. The coupling efficiencies of different input radial modes (from LG_0^0 to LG_3^0) for various pairs of phase screens formed the "crosstalk matrix." It should be noted that we include the LG_0^0 mode in our basis set for completeness and for examining the crosstalk.

Figure 4 shows the calculated intensities and phase fronts of different input modes (LG_0^0, LG_1^0, LG_2^0, and LG_3^0) at the Fourier plane after the application of phase screens calculated for the LG_2^0 mode. Essentially, one obtains nearly Gaussian amplitude and a flat phase at the Fourier plane only when the applied phase screens correspond to the particular input mode.
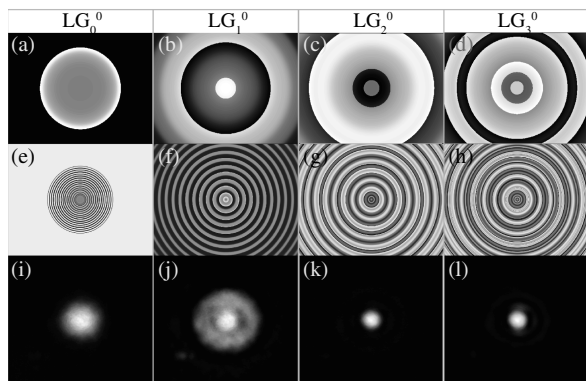

Fig. 3. (a)–(d) Phase screens on SLM1 and (e)–(h) on SLM2 for input radial modes LG_0^0 to LG_3^0 (from left to right). In calculating these phase screens, the GS algorithm was applied for 200 iterations (well beyond the stagnation point). (j)–(l) Captured intensities at SLM2 after applying the corresponding phase screens to the various input modes LG_0^0 to LG_3^0 (from left to right). In all cases, the transformed intensity closely resembles the near-Gaussian mode of a SMF, although some distortion is evident in panel (j).
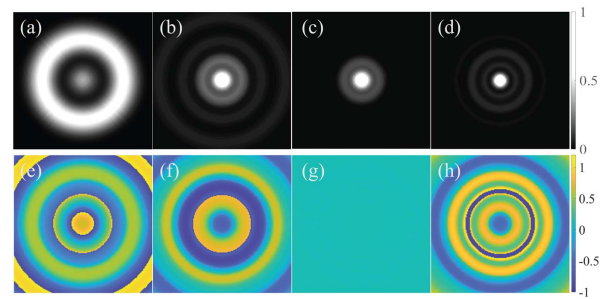

Fig. 4. Calculated (a)–(d) intensities and (e)–(h) phases of input modes LG_0^0 to LG_3^0 (from left to right) at the Fourier plane after the application of phase corrections corresponding to LG_2^0 mode. The intensities are normalized to the maximum intensity, and the phases are given in units of π radians. Note that only when the input mode corresponds to the phase screens on the two SLMs does the transformed mode have the correct amplitude (c) and (flat) phase (g) distributions to couple to the Gaussian mode profile of a single-mode fiber.

Since the coupling efficiency of the transformed modes to the SMF depends on both intensity and phase distributions, the improperly transformed modes have negligible coupling efficiency to the SMF (or equivalently, negligible crosstalk). Hence, the coherent mode-overlap efficiency, or C in Eq. (1), between the transformed modes and the SMF mode is the pertinent measure for the efficacy of these phase screens.

Figure 5(a) shows the predicted crosstalk matrix, which is obtained by calculating the overlap integral of each transformed radial mode with the SMF mode for different pairs of phase screens. The diagonal elements of the matrix have high values (larger than 0.8), implying high conversion efficiency for the radial modes with the correct pair of phase screens. The off-diagonal elements, on the other hand, have low values (less than 0.02), implying negligible crosstalk. Further, in agreement with Fig. 1(b), the conversion efficiency of radial modes [diagonal elements of Fig. 5(a)] decreases monotonically with increasing radial index, from 99% for LG_0^0 to approximately 81% for LG_3^0. We also obtain theoretical mutual information ($I_{p_{in}, p_{screen}}$) of 1.6812 bits per transmitted photon, which is close to 2, the maximum for a four-dimensional space. In contrast, for the phase-and-intensity flattening method of [25], $I_{p_{in}, p_{screen}}$ was significantly lower at 0.134194. Comparing the diagonal terms of the measured crosstalk matrix [shown in Fig. 5(b)] with 5(a), we see that the coupling efficiencies for all the modes, with the correct pair of phase screens is lower than the calculated result. Also, except for LG_3^0 (or $p_{in} = 3$), the measured crosstalk values
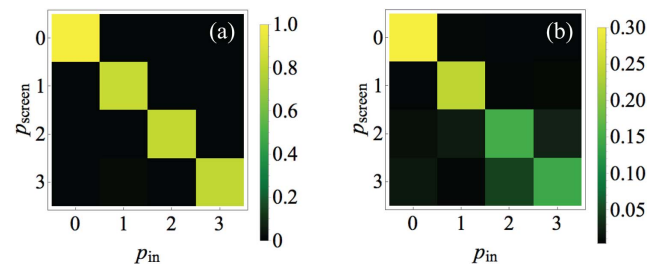

Fig. 5. Crosstalk matrices (a) from calculations and (b) obtained experimentally. Here, p_{in} is the radial index of the input mode, whereas p_{screen} is the radial index corresponding to the pair of phase screens. See Data File 2 for the actual values.

(or the off-diagonal terms) are less than 15%. In addition, although not shown here, the crosstalk degrades substantially (greater than 60%) for mode LG_4^0 onwards.

The lower coupling efficiency measured overall, and the observed crosstalk for radial indices larger than 1 could be due to a combined effect of the following factors: (1) calibration errors at each pixel on the SLMs (correct calibration of each pixel is a stringent requirement for SLM2; SLM1 has a grating for mode generation, and, therefore, any calibration errors therein would manifest in diffraction efficiency, and not as significantly in the profile of the generated mode); (2) imperfect optics, and the presence of residual aberrations such as astigmatism and spherical aberration in the imaging systems before and after SLM2; and (3) crosstalk between the pixels on the SLMs (called the fringing effect in [34]), which becomes significant whenever the phase wraps from 2π to 0 gradually over a few pixels instead of sharply. A possible solution for improving the coupling efficiency and lowering the crosstalk could be to use a genetic algorithm similar to the one used in [28] to calibrate and correct for the phase errors due to the SLMs as well as the imaging systems accurately. Also, a hologram with high spatial resolution should reduce the crosstalk between adjacent pixels during phase wrapping.

To summarize, we have proposed and provided a proof-of-principle demonstration of a new protocol for determining the radial mode decomposition of an optical field. The protocol utilizes two phase transformations, one at the object and the other in the Fourier plane of a lens, to convert high-order radial modes to the fundamental mode of a SMF. The required phase transformations were calculated through the use of the GS algorithm. The implementation is straightforward and does not require complicated setups or optimization. Also, as it utilizes only phase corrections, our procedure for maximizing the coherent mode overlap between the high-order LG modes and the Gaussian mode is intrinsically non-lossy. We believe that by improving on the implementation, as suggested in the preceding paragraph, the performance can be improved further.

The universal nature of the phase-retrieval algorithm suggests the future use of this protocol for measurements of the azimuthal mode structure in addition to the radial modes, or for measurements in other bases, including the Hermite–Gaussian basis. One can essentially increase the dimensionality of space-division multiplexing in communication [7] through the use of this protocol, or integrate it with other available mode-sorting techniques to perform high-dimensional QKD, as very recently done in [35]. In addition, this protocol may be useful for applications such as super-resolution [36] and quantum state tomography [12,23].

REFERENCES

1. L. Allen, M. W. Beijersbergen, R. J. C. Spreeuw, and J. P. Woerdman, Phys. Rev. A **45**, 8185 (1992).
2. W. N. Plick and M. Krenn, Phys. Rev. A **92**, 063841 (2015).
3. P. W. Milonni and J. H. Eberly, *Laser Physics* (Wiley, 2010), pp. 269–329.
4. J. Wang, J. Y. Yang, I. M. Fazal, N. Ahmed, Y. Yan, H. Huang, Y. Ren, Y. Yue, S. Dolinar, M. Tur, and A. E. Willner, Nat. Photonics **6**, 488 (2012).
5. N. Bozinovic, Y. Yue, Y. Ren, M. Tur, P. Kristensen, H. Huang, A. E. Willner, and S. Ramachandran, Science **340**, 1545 (2013).
6. A. E. Willner, H. Huang, Y. Yan, Y. Ren, N. Ahmed, G. Xie, C. Bao, L. Li, Y. Cao, Z. Zhao, J. Wang, M. P. J. Lavery, M. Tur, S. Ramachandran, A. F. Molisch, N. Ashrafi, and S. Ashrafi, Adv. Opt. Photon. **7**, 66 (2015).
7. G. Xie, Y. Ren, Y. Yan, H. Huang, N. Ahmed, L. Li, Z. Zhao, C. Bao, M. Tur, S. Ashrafi, and A. E. Willner, Opt. Lett. **41**, 3447 (2016).
8. G. Gibson, J. Courtial, M. J. Padgett, M. Vasnetsov, V. Pas'ko, S. M. Barnett, and S. Franke-Arnold, Opt. Express **12**, 5448 (2004).
9. M. Mirhosseini, O. S. Magaña-Loaiza, M. N. O'Sullivan, B. Rodenburg, M. Malik, M. P. J. Lavery, M. J. Padgett, D. J. Gauthier, and R. W. Boyd, New J. Phys. **17**, 033033 (2015).
10. A. Sit, F. Bouchard, R. Fickler, J. Gagnon-Bischoff, H. Larocque, K. Heshami, D. Elser, C. Peuntinger, K. Günthner, B. Heim, C. Marquardt, G. Leuchs, R. W. Boyd, and E. Karimi, Optica **4**, 1006 (2017).
11. M. Bourennane, A. Karlsson, G. Björk, N. Gisin, and N. J. Cerf, J. Phys. A Math. Gen. **35**, 10065 (2002).
12. M. Krenn, M. Huber, R. Fickler, R. Lapkiewicz, S. Ramelow, and A. Zeilinger, Proc. Natl. Acad. Sci. USA **111**, 6243 (2014).
13. M. Mirhosseini, M. Malik, Z. Shi, and R. W. Boyd, Nat. Commun. **4**, 2781 (2013).
14. G. C. G. Berkhout, M. P. J. Lavery, J. Courtial, M. W. Beijersbergen, and M. J. Padgett, Phys. Rev. Lett. **105**, 153601 (2010).
15. J. Leach, J. Courtial, K. Skeldon, S. M. Barnett, S. Franke-Arnold, and M. J. Padgett, Phys. Rev. Lett. **92**, 013601 (2004).
16. E. Karimi, B. Piccirillo, E. Nagali, L. Marrucci, and E. Santamato, Appl. Phys. Lett. **94**, 231124 (2009).
17. T. Su, R. P. Scott, S. S. Djordjevic, N. K. Fontaine, D. J. Geisler, X. Cai, and S. J. B. Yoo, Opt. Express **20**, 9396 (2012).
18. A. Mair, A. Vaziri, G. Weihs, and A. Zeilinger, Nature **412**, 313 (2001).
19. R. Ionicioiu, Sci. Rep. **6**, 25356 (2016).
20. Y. Zhou, M. Mirhosseini, D. Fu, J. Zhao, S. M. Hashemi Rafsanjani, A. E. Willner, and R. W. Boyd, Phys. Rev. Lett. **119**, 263602 (2017).
21. X. Gu, M. Krenn, M. Erhard, and A. Zeilinger, Phys. Rev. Lett. **120**, 103601 (2018).
22. D. Fu, Y. Zhou, R. Qi, S. Oliver, Y. Wang, S. M. H. Rafsanjani, J. Zhao, M. Mirhosseini, Z. Shi, P. Zhang, and R. W. Boyd, "Realization of a scalable Laguerre-Gaussian mode sorter based on a robust radial mode sorter," arXiv:1809.10319 (2018).
23. B. Jack, J. Leach, H. Ritsch, S. Barnett, M. Padgett, and S. Franke-Arnold, New J. Phys. **11**, 103024 (2009).
24. H. Qassim, F. M. Miatto, J. P. Torres, M. J. Padgett, E. Karimi, and R. W. Boyd, J. Opt. Soc. Am. B **31**, A20 (2014).
25. F. Bouchard, N. H. Valencia, F. Brandt, R. Fickler, M. Huber, and M. Malik, "Measuring azimuthal and radial modes of photons," arXiv:1808.03533 (2018).
26. J. F. Morizur, L. Nicholls, P. Jian, S. Armstrong, N. Treps, B. Hage, M. Hsu, W. Bowen, J. Janousek, and H. Bachor, J. Opt. Soc. Am. A **27**, 2524 (2010).
27. N. K. Fontaine, R. Ryf, H. Chen, D. Neilson, K. Kim, and J. Carpenter, "Laguerre-Gaussian mode sorter," arXiv:1803.04126 (2018).
28. R. Fickler, M. Ginoya, and R. W. Boyd, Phys. Rev. B **95**, 161108 (2017).
29. J. R. Fienup, Proc. SPIE **373**, 147 (1984).
30. R. W. Gerchberg and W. O. Saxton, Optik **35**, 237 (1972).
31. J. R. Fienup, Appl. Opt. **21**, 2758 (1982).
32. J. Seldin and J. R. Fienup, J. Opt. Soc. Am. A **7**, 412 (1990).
33. V. Arrizón, U. Ruiz, R. Carrada, and L. A. González, J. Opt. Soc. Am. A **24**, 3500 (2007).
34. T. Lu, M. Pivnenko, B. Robertson, and D. Chu, Appl. Opt. **54**, 5903 (2015).
35. Y. Zhou, M. Mirhosseini, S. Oliver, J. Zhao, S. M. H. Rafsanjani, M. P. J. Lavery, A. E. Willner, and R. W. Boyd, "High-dimensional free-space quantum key distribution using spin, azimuthal, and radial quantum numbers," arXiv:1809.09986 (2018).
36. M. Tsang, R. Nair, and X. M. Lu, Phys. Rev. X **6**, 031033 (2016).